Temperature-concentration phase diagram of *P*2-Na_xCoO_2 from first-principles calculations

Yoyo Hinuma (日沼洋陽),[1] Ying S. Meng (孟穎),[1,2] and Gerbrand Ceder[1,*]

[1]*Department of Materials Science and Engineering, Massachusetts Institute of Technology, 77 Massachusetts Avenue, Cambridge, Massachusetts 02139, USA*

[2]*Department of Materials Science and Engineering, University of Florida, 135 Rhines Hall, Gainesville, Florida 32611, USA*

(Received 14 January 2008; published 23 June 2008)

Temperature-concentration phase diagrams for Na_xCoO_2 ($0.5 \leq x \leq 1$) are obtained by combining density functional theory (DFT) in the generalized gradient approximation (GGA) and in the GGA with Hubbard U correction (GGA+U) with the cluster expansion and Monte Carlo simulation technique. In the GGA, holes are delocalized over the Co layer, while in GGA+U the charges on the Co layer completely localize, forming distinct Co^{3+} and Co^{4+} cations. The leading interactions in GGA are long-range in-plane electrostatics and relaxation effects, whereas in GGA+U Co-Co interactions dominate. Comparison of ground states, c-lattice parameter, and Na1/Na2 ratio with experimental results consistently suggests that GGA is a better approximation for $0.5 \leq x \leq 0.8$.

DOI: 10.1103/PhysRevB.77.224111 PACS number(s): 61.66.Fn, 64.60.Ej

I. INTRODUCTION

Sodium cobaltate (Na_xCoO_2) is a material with exceptional electronic and magnetic properties. At high sodium concentrations a remarkable combination of high electronic conductivity and high Seebeck coefficient[1,2] is observed, while hydrated Na_xCoO_2 with low sodium content is a superconductor.[3] The structure of these materials is of particular importance as mixed Co^{3+}/Co^{4+} systems are often close to a localization and/or delocalization transition.[4] Minor deviations of the local electrostatic potential on Co, such as those induced by local Na^+ order or disorder, may therefore significantly influence the electronic state. In this work, we use an *ab initio* computational approach to study Na-vacancy ordering in the two-layer *P*2-Na_xCoO_2 (γ-Na_xCoO_2, $0.5 \leq x \leq 1$) system as a function of temperature and composition. By using different electronic structure methods within density-functional theory [generalized gradient approximation (GGA) to density-functional theory (DFT) and the GGA with Hubbard U correction (GGA+U)], we can investigate the effect of Co-charge localization and ordering of Na and vacancies.

Na_xCoO_2 in the *P*2 structure can be thought of as a layered structure with close-packed oxygen layers alternating with either Na or Co layers. "*P*2" refers to the notation of layered structures as first introduced by Delmas *et al.*[5] whereby the first letter ("*O*," "*T*," or "*P*") refers to the nature of the site occupied by the alkali ion (octahedral, tetrahedral, or prismatic), and "2" refers to the number of alkali layers in the repeat unit perpendicular to the layering. Figure 1(a) is a perspective on the structure along the layers showing how the layers are stacked. The oxygen ions (black small spheres in Fig. 1) stack as *ABBA*|*ABBA*, which is referred as *P*2 after the notation introduced by Delmas *et al.*[5] Co (gray small spheres in Fig. 1) occupies the octahedral sites between the *AB* arranged oxygen layers, while Na occupies prismatic sites between the *BB* (or *AA*) arranged oxygen layers. Na can occupy two types of sites: The oxygen prism of the Na1 site shares its top and bottom faces with CoO_6 octahedra and the oxygen prism around the Na2 sites shares edges with CoO_6 octahedra. Together, the Na1 and Na2 sites form a honeycomb lattice. Figure 1(b) shows a top view of Na_xCoO_2. Note that the Na2 sites in two adjacent layers are shifted due to the *P*2 (*AABB*) stacking of oxygen ions. It is unlikely that the nearest Na1 and Na2 sites are occupied simultaneously to avoid overlapping of ions, as they are only about 1.63 Å apart in $Na_{0.5}CoO_2$,[6] which is less than two times the ionic radius of Na. One would expect that the Na1 site is less preferred than the Na2 site as the Na^+-$Co^{3+/4+}$ distance is smaller in the former.[7]

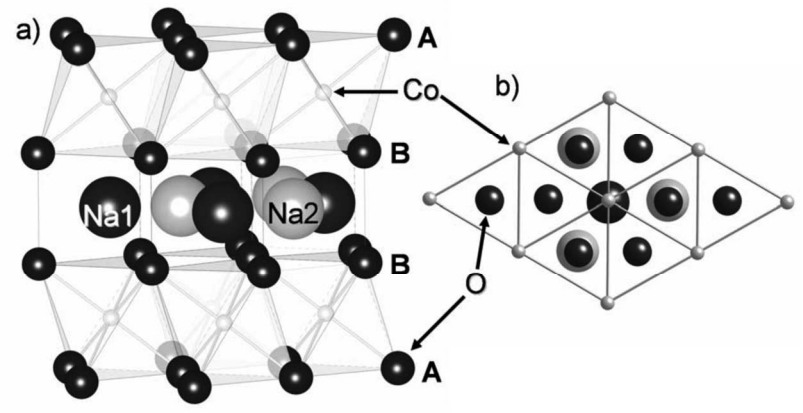

FIG. 1. Two perspectives of the layered *P*2-Na_xCoO_2 structure. (a) View perpendicular to the layers to show the oxygen stacking. (b) Top view to show relative positions of Na1, Na2, Co, and oxygens.

$P2$-Na_xCoO_2 can be made with any Na concentration between $0.64<x<0.74$ by direct powder synthesis.[8] Chemical[6,9] or electrochemical[8,10] Na removal and/or intercalation from Na_xCoO_2 can be used to form $P2$-Na_xCoO_2 with other compositions. Since Na^+ removal is compensated by a change in electron concentration in the Co-O electronic states, $P2$-Na_xCoO_2 is an excellent system to study the relations between crystal structure, electronic structure, and properties.

Despite the enormous interest in $P2$-Na_xCoO_2, its structure as a function of Na concentration is not fully characterized. Experimental[10–14] and theoretical[11,15–17] work has led to proposed structures for several Na-vacancy ordered states. The ground-state ordering of $Na_{0.5}CoO_2$ has been determined experimentally with electron diffraction[12,14] and is in agreement with results from first-principles calculations.[15,16] Based on experiments three ordering schemes are proposed at the composition $Na_{0.75}CoO_2$, namely, the "droplet" phase by Roger *et al.*[11] from neutron diffraction with $2\sqrt{3}a_{hex} \times 2\sqrt{3}a_{hex}$ ordering and formation of isolated three-Na1 droplet motifs, the "stripe" phase by Geck *et al.*[13] from high energy x-ray diffraction with $2a_{hex} \times 2\sqrt{3}a_{hex}$ ordering and formation of three-Na1 and three-Na2 droplet motifs that are connected by two corners each to droplets of the same type, and the "diamond" phase by Zandbergen *et al.*[12] from electron diffraction with $4a_{hex} \times \sqrt{3}a_{hex}$ ordering and formation of connected diamond such as Na1 and Na2 motifs. The "diamond" phase is also computationally suggested as a ground state by Zhang *et al.*,[16] however, detailed first-principles calculations by Meng *et al.*[17] show that a different "zigzag" structure with $4a_{hex} \times \sqrt{3}a_{hex}$ ordering where Na1 orders in a zigzag pattern has lower energy. At higher compositions, such as $x>0.85$, six-Na1 droplet patterns,[15,18] analogous to the three-Na1 droplet motifs by Roger *et al.*,[11] are suggested by computation.

Understanding and predicting the Na-vacancy ordering is complicated by the fact that the Co ions have an average valence between +3 and +4, and the nature of this mixed-valence state is under considerable dispute. Whether or not charge localizes on Co and forms distinct Co^{3+} and Co^{4+} ions is an important issue that will affect Na-vacancy ordering. Bond length analysis from neutron diffraction shows delocalization of Co charge in $Na_{0.5}CoO_2$;[6] however, magnetic-susceptibility and conductivity measurements suggest that at low temperatures $Na_{0.5}CoO_2$ is a charge-ordered insulator.[19] Magnetic susceptibility and conductivity measurements also suggest that Na_xCoO_2 is a Curie–Weiss metal at $0.5<x<0.75$ and is in a weak-moment magnetically ordered state at $x \geq 0.75$, possibly because of spin-density waves. Specifically, at $x=0.65$ (Ref. 20) and $\sim 2/3$ (Ref. 19), these measurements imply delocalization of Co charge. On the other hand, partial localization of Co charge is suggested at $x=0.75$ based on observation of a magnetic transition[21] and from the results of muon spin rotation and relaxation[22] and neutron scattering[23] measurements. At $x=0.82$, the presence of superstructures with antiferromagnetic ordering observed by neutron-scattering measurements also suggests partial localization of charge on Co.[24] Band calculations on $Na_{0.5}CoO_2$ in the local-spin-density approximation by Singh[25] suggest a ferromagnetic instability of itinerant half-metallic character, and a delicate insulating phase is observed by band calculations on $Na_{0.5}CoO_2$ using the local-density approximation with Hubbard U correction (LDA+U) by Lee and Pickett.[26] Both delocalized and localized Co^{4+} holes exist depending on the local Na arrangement. Some evidence exists for a strong coupling between the Na positions and charge on the Co ion. Marianetti and Kotliar[7] proposed a computational model within the dynamic mean field theory (DMFT) in which a Co^{4+} hole that is nearest neighbor to a Na1 is penalized by 400 meV. Hence the occupancy of the Na1 sites in this model reduces the number of Co ions over, which holes can delocalize and encourages Co^{4+} localization. Comparing results from the GGA and GGA+U methods, Huang *et al.*[14] showed that at $Na_{0.75}CoO_2$, the Na-vacancy ordering is strongly coupled with Co^{3+}/Co^{4+} charge ordering.

Phase transition temperatures of Na_xCoO_2 have been experimentally measured at key compositions. At $x=0.5$, electronic and magnetic transitions have been observed at 87, 53, and 20 K.[14] Structural transitions at 210 and 410–470 K have been observed by electron diffraction,[27] and incipient localization of holes is reported to be evident at 300 K.[19] At $x=0.75$, a magnetic ordering is found below 22 K,[28] and resistivity transitions are observed at approximately 285 and 315 K.[11] At $x=0.65$, no magnetic transition has been found down to 2 K.[28]

Experimentally it is difficult to obtain the exact stoichiometry. Chou *et al.*[29] pointed out the possibility of oxygen nonstoichiometry in Na_xCoO_2 on single crystals prepared with the floating zone method. $Na_{0.75}CoO_2$ prepared with the floating zone method was observed to cross two tie lines upon heating close to 1020 °C. Oxygen deficiency levels of $\delta \sim 0.073$ was observed in $Na_{0.7}CoO_{2-\delta}$ prepared in air[30] and $\delta \sim 0.08$ was observed in $Na_{0.75}CoO_{2-\delta}$ prepared in an oxygen atmosphere.[29] Oxygen deficiency is important as it modifies the relation between the Na content and the average Co-valence. In addition, for example, in samples prepared with the floating zone method, CoO_x formation has been suggested both by magnetic-susceptibility measurement[31] and differential thermal analysis.[29] Samples with Na concentration lower than $x=0.7$ are usually prepared by removal of Na with I_2 from $Na_{0.75}CoO_2$,[6,9] and in this case, composition control of the final product is very difficult. Electrochemical methods to alter the Na content[8,10] offer better control provided that the composition of the initial compound is accurately determined.

In this paper, we used *ab initio* methods to study the temperature-composition phase diagram of $P2$-Na_xCoO_2 for $x>0.5$. The dependence of the energy on Na-vacancy configuration (or Co^{3+}/Co^{4+} configuration) is expanded using the cluster expansion technique[32–49] so that Monte Carlo simulations can be used to equilibrate the system at nonzero temperature. We use both the GGA and GGA+U for the phase diagram construction, allowing us to understand how charge localization on Co affects the Na-vacancy ordering. The objective of this paper is to computationally obtain the key interactions in this material, the ordered states, and their transition temperatures at different Na concentrations and to gain an understanding of the role that possible $Co^{3+/4+}$ charge localization plays on the phase diagram.

II. METHODOLOGY

A. First-principles calculations

Our approach is to use the well-established cluster expansion approach to the prediction of phase diagrams from first principles.[32–49] The cluster expansion parameterizes the energy of the system as a function of the occupation of the sites on which the configurational disorder problem is defined. In this case the cluster expansion is defined on the possible sites of the Na sublattice as well as on the Co sublattice (for the GGA+U approach only). The cluster expansion captures the accurate energies of the DFT calculations, and a finite temperature behavior of the system is sampled with Monte Carlo simulations.

First-principles calculations on various ordered arrangements were performed in the spin-polarized GGA or GGA+U method. Core electron states were represented by the projector augmented-wave method[50] as implemented in the Vienna *Ab Initio* Simulation Package (VASP).[51] All Co^{4+} spins were initialized ferromagnetically. Co^{3+} has no net spin as it is low spin in these materials. The Perdew–Burke–Ernzerhof exchange correlation[52] and a plane-wave representation for the wave function with a cutoff of 450 eV were used. Both internal coordinates and unit-cell lattice parameters were fully relaxed, unlike in previous work,[13,15,16] where the unit-cell lattice parameters were fixed. Full relaxation has been reported to be crucial in identifying the correct order of phase stability.[18] The Brillouin zones were sampled with a mesh including the gamma point. The density of the mesh for all calculations is approximately one point per 0.01 $Å^{-3}$. In the GGA+U calculations, the Hubbard U value in the Hamiltonian ($U_{\text{eff}}=U-J$, or afterward simply U) is taken to be 5 eV for Co. This value for U is between the values of $U=4.91$ eV for Co^{3+} and $U=5.37$ eV for Co^{4+} obtained with first-principles perturbation theory in Li_xCoO_2.[53] While GGA+U (or LDA+U) is most often used to open up a Hubbard gap in the electronic structure, it was previously shown that in related systems it also has a significant and meaningful effect on the energy. As it removes the self-interaction in the metal d orbitals, it leads to strong charge localization, significant changes in the ground-state structures,[54–56] and more accurate redox energies.[53,57] A value of $U=5$ eV is sufficient to cause hole localization in $Na_{0.5}CoO_2$ (Ref. 58) and is consistent with our previous work on $Na_{0.75}CoO_2$,[17] but slightly higher than the value in the work by Wang *et al.*[15] ($U=4$ eV). The rotationally invariant approach to GGA+U by Liechtenstein *et al.*[59] was used for calculations in this work for consistency with previous work,[17] different from the rotationally invariant approach by Dudarev *et al.*[60] used by Wang and Ni.[15]

B. Cluster expansion

To model partially disordered states at finite temperatures, the cluster expansion method is used. This methodology is well established for alloys[39–47] and has previously been used to study Li and/or vacancy disorder in layered systems, such as Li_xCoO_2,[32,48,49] Li_xNiO_2,[33] and $Li_xNi_{0.5}Mn_{0.5}O_2$.[34,35] In the Na_xCoO_2 system, the Na sites are described by a lattice model, with variables describing whether Na or a vacancy sits on each site. The essential idea is to expand the energy of the system in terms of these variables. For the GGA approximation, using the occupation variables $\sigma=1$ for Na and $\sigma=-1$ for vacancies for Na sites, the Hamiltonian becomes

$$E_v^{\text{predict}} = C + \sum_{i\in \text{Na1 site}} V^{\text{Na1}}\sigma_i + \sum_{i\in \text{Na2 site}} V^{\text{Na2}}\sigma_i + \sum_{i,j} V^{ij}\sigma_i\sigma_j + \sum_{i,j,k} V^{ijk}\sigma_i\sigma_j\sigma_k + \cdots . \quad (1)$$

Here, E_n^{predict} is the predicted energy for structure ν, C is a constant, and V are the effective cluster interactions (ECI). The point terms are broken out explicitly in Na1-type and Na2-type sites in Eq. (1). The energy difference of Na on Na1 and Na2 sites, averaged over all possible occupations surrounding the sites is given by $2(V^{\text{Na1}}-V^{\text{Na2}})$. The indices i, j, and k are labels of sites in the interaction cluster.

In the GGA+U approximation, the additional problem of organizing charge occupancy on Co^{3+}/Co^{4+} appears, and the Na and/or vacancy and Co^{3+}/Co^{4+} sublattices interact with each other. Such a system with two partially disordered sublattices, which interact with each other can be studied with a coupled cluster expansion.[35,36,61] A coupled cluster expansion is essentially an expansion in the product basis of the configurational functions (clusters) defined on each sublattice.[62] A similar approach was recently used to capture the interaction between disorder of Li and/or vacancy and Fe^{2+}/Fe^{3+} disorder in Li_xFePO_4.[36] The GGA+U cluster expansion Hamiltonian becomes

$$E_v^{\text{predict}} = C + \sum_{i\in \text{Na2 site}} V^{\text{Na2}}\sigma_i + \sum_{i\in \text{Co site}} V^{\text{Co}}\tau_i + \sum_{i,j} V^{ij}\sigma_i\sigma_j + \sum_{i,j} V^{ij}\sigma_i\tau_j + \sum_{i,j} V^{ij}\tau_i\tau_j + \sum_{i,j,k} V^{ijk}\sigma_i\sigma_j\sigma_k + \sum_{i,j,k} V^{ijk}\sigma_i\sigma_j\tau_k + \sum_{i,j,k} V^{ijk}\sigma_i\tau_j\tau_k + \sum_{i,j,k} V^{ijk}\tau_i\tau_j\tau_k + \cdots , \quad (2)$$

where the occupation variables are $\sigma=1$ for Na and $\sigma=-1$ for vacancies at Na sites, and $\tau=1$ for Co^{3+} and $\tau=-1$ for Co^{4+} at Co sites. Note that due to the charge balance constraint,

$$\sum_{i\in \text{Na1 site}} \sigma_i + \sum_{i\in \text{Na2 site}} \sigma_i - \sum_{i\in \text{Co site}} \tau_i = \text{const}, \quad (3)$$

one interaction term for a point variable must be removed. In our cluster expansion, the ECI for the Na1 point term was removed. Hence the point ECI for Na2 and Co^{3+}/Co^{4+} are taken with respect to this term.

While in principle the expansion of Eqs. (1) and (2) has to be summed over all pairs, triplets, quadruplets, and larger clusters of sites, in practice relevant cluster interactions can be selected on the basis of how well they minimize the weighted Cross-Validation (CV) score, which is a means of measuring how good the cluster expansion is at predicting the energy of a structure not included in the fit.[63] Truncation amounts to neglecting the effect of configurational details beyond a certain range on the energy, and only taking the average interaction into account. The cluster expansion is

obtained through an iterative approach, whereby energies of newly predicted ground-state candidate structures and other relevant structures suggested by previous cluster expansions are added into the training set of energies and structures used to fit the ECIs. The final GGA cluster expansion was fitted to the energies of 211 different Na-vacancy configurations, and the final GGA+U cluster expansion was fitted to the energies of 131 different Na-vacancy and Co^{3+}/Co^{4+} configurations in the concentration range $0.5 \leq x \leq 1$. The maximum size of the unit cell is 42 f.u. in GGA and 40 f.u. in GGA+U. One f.u. contains one Co unit. Structures with different shape and size were calculated to search for ground states. In GGA +U, both the Na-vacancy and Co^{3+}/Co^{4+} configurations were independently changed, although charge neutrality was maintained. Although automated schemes to find relevant structures to include in the cluster expansion training set exist, such as in the MAPS code,[63] structures were picked "by hand." Structures similar to those with energies on or close to the convex hull were investigated in detail and were more heavily weighted in obtaining the CV score.

In the GGA cluster expansion, to capture the slowly decaying long-range electrostatic interactions in the Na layers, it was necessary to subtract a "background cluster expansion" prior to fitting the first-principles energies to the cluster expansion. The background cluster expansion is defined as

$$E'_v = \sum_{\text{In-plane pair}} V'_{ij}\sigma_i\sigma_j, \tag{4}$$

with

$$V'_{ij} = A\frac{\text{erfc}(\alpha r_{ij})}{\alpha r_{ij}}. \tag{5}$$

Here, r_{ij} is the distance in angstroms between two sites i and j forming the pair cluster. A (magnitude) and α (decay length) are constants that are manually chosen. The background interaction V'_{ij} has the same form as the real-space term in an Ewald summation, which was shown to reproduce well low-energy structures in ionic systems governed by unscreened electrostatic interactions.[64]

The cluster expansion in Eq. (1) is fitted to energies $E_{\text{GGA},\nu} - E'_\nu$ instead of directly fitting to first-principles energies $E_{\text{GGA},\nu}$. The phase space for which first-principles energies can be obtained is limited since Na1-Na2 nearest-neighbor (NN) simultaneous occupancy cannot be stabilized in both GGA and GGA+U approximations due to overlapping of ions, and Na1-Co^{4+} NN simultaneous occupancy drastically increases the energy in the GGA+U approximation due to strong electrostatic repulsion. Therefore, clusters that include the Na1-Na2 NN pair cluster or Na1-Co NN pair cluster (in the GGA+U cluster expansion) as a subcluster were not included in the cluster expansion. To discourage the formation of such pairs in the Monte Carlo simulations, a penalty of 1 eV per Na1-Na2 NN simultaneous occupancy and 400 meV per Na1-Co^{4+} NN simultaneous occupancy was added. The exact magnitude of the Na1-Na2 NN pair penalty is not important since as long as these configurations do not appear in the simulation they do not affect the value of the average energy. However, since there is no overlap of ions involved, there is no reason to limit Na1-Co^{4+} NN simultaneous occupancy in Monte Carlo simulations at high temperatures, and the magnitude of this penalty is chosen to be the same as the value in Marianetti and Kotliar.[7] A cluster expansion that involves penalties to limit accessible phase space was previously implemented in the $LiNi_{0.5}Mn_{0.5}O_2$ system.[35]

C. Monte Carlo simulations

Grand Canonical Monte Carlo simulations with the Metropolis algorithm[65] were conducted for both the GGA and GGA+U based cluster expansion to investigate ground states and obtain phase diagrams. Monte Carlo cells with up to approximately 30 000 Na sites (15 000 f.u.) were used. For the cluster expansion based on the GGA approximation, 80 000 equilibrium passes and 120 000 sampling passes were used at 10 K intervals for calculations at fixed chemical potential, and at least half the number of passes were used when the chemical potential was scanned at fixed temperature. The perturbation in the Metropolis algorithm was a sign inversion of the occupation variable in one site, and one sampling pass amounts to one possible perturbation for each site on the lattice.

In the GGA+U calculations, 40 000 equilibrium passes and 60 000 sampling passes were used at 10 K intervals for temperature scans at fixed chemical potential, and half this number of passes for chemical-potential scans at fixed temperature. The perturbation for the Metropolis algorithm was chosen with the following algorithm to ensure charge balance.

(1) Choose a first site randomly.

(2) Choose a second site randomly.

(3) If inverting the occupation variables in both sites changes the charge balance, discard the choice of the second site and go to (2).

(4) Else, the perturbation is inverting the occupation variables in both sites.

One sampling pass amounts to one possible selection as the first candidate site for inversion per site on the lattice. Some phase-transition temperatures are obtained by looking at discontinuities in concentration or formation energies, while transition temperatures that cannot be determined by visual inspection of discontinuities, such as when there is significant hysterisis, are obtained by free-energy integration. The free energy $\Phi(T,\mu) = \langle E\rangle - TS - \mu\langle N\rangle$ can be calculated by the integration $\Phi(T_0,\mu) = \Phi(T_0,\mu_0) - \int_{\mu_0}^{\mu}\langle N(T_0,\mu)\rangle d\mu$ on a fixed temperature trajectory, or $\Phi(T,\mu_0)/kT = \Phi(T_0,\mu_0)/kT_0 + \int_{T_0}^{T}\{\langle E(T,\mu_0)\rangle - \mu\langle N(T,\mu_0)\rangle\}d\beta$ on a fixed chemical-potential trajectory. Here, T is the temperature, μ is the chemical potential, N is the concentration, $\beta = 1/kT$, and k is the Boltzmann constant. The free energy for ordered phases are obtained by integrating the grand canonical energy $\langle E\rangle - \mu\langle N\rangle$ from low temperature on a fixed chemical-potential trajectory. The free energy for the disordered phase is obtained by first integrating the concentration $\langle N\rangle$ from $x = 1$ over chemical potential at a temperature, which is above the order-disorder temperature for all ordered phases (650 K for GGA and 750 K for GGA+U calculations) and then in-

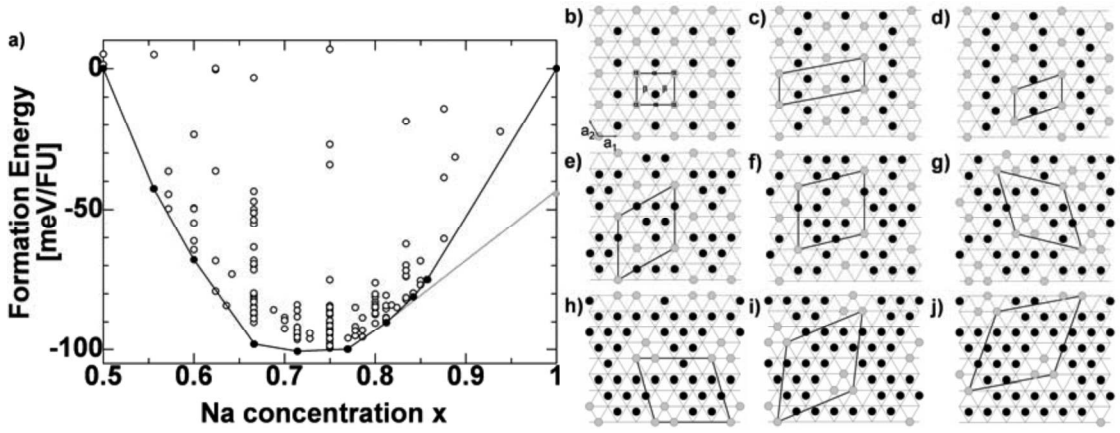

FIG. 2. (a) First principles GGA formation energy per formula unit. The bold solid line shows the convex hull. The convex hull changes to the dotted line when formation of $O3$-$NaCoO_2$ (gray diamond) is allowed. [(b)–(j)] In-plane ordering of the GGA ground states at (b) $x=0.5$, (c) 0.56 (5/9), (d) 0.6, (e) 0.67 (4/6), (f) 0.71 (5/7), (g) 0.77 (10/13), (h) 0.81 (13/16), (i) 0.84 (16/19), and (j) 0.86 (18/21), respectively. Legend: gray circles, Na1 and black circles, Na2. The bold lines indicate unit cell. The symbols α and β in (b) indicate the distinction of α and β sites for order-parameter calculation on the Na1 sublattice.

tegrating $\langle E\rangle-\mu\langle N\rangle$ over temperature with fixed chemical potential. Brackets indicate thermodynamically averaged quantities.

III. RESULTS

A. Generalized gradient approximation

1. Formation energies and ground states

Figure 2(a) shows the GGA formation energy per f.u., which is the energy of a structure compared to phase separation into the lowest-energy structures with $P2$ stacking at $x=0.5$ and $x=1$. A large number of structures close to the convex hull were calculated since it is crucial to obtain the correct ground states and to accurately obtain the energy scale of the low-energy excitations to compile an accurate phase diagram. Some structures with large excitation energies are also necessary to "pin" such structures at high energy in the cluster expansion so their local environments of high-energy structures do not form in the Monte Carlo simulations.

The dotted line in Fig. 2(a) shows the convex hull when $O3$-$NaCoO_2$ (shown with the gray diamond) is considered as an end member. $O3$-$NaCoO_2$ is the ground state for $NaCoO_2$,[66] where oxygen ions are stacked as $ABCABC$ and Na and Co occupy octahedral sites in alternating layers; its energy is 45 meV/f.u. lower than that of $P2$-$NaCoO_2$. This is why even in electrochemical experiments it is difficult to obtain single phase $P2$-Na_xCoO_2 with Na concentrations above $x>0.8$. When $O3$-$NaCoO_2$ is added on the convex hull, two ground states at $x\sim0.84$ and 0.86 are removed from the convex hull.

Figures 2(b)–2(j) show in-plane Na ordering patterns of the ground state. The ground states can be grouped into three types of ordering patterns:[18] The "row" pattern for $x=0.5$ [=2/4, Fig. 2(b)],[12,14] 0.56 [=5/9, Fig. 2(c)], and 0.6 [=3/5, Fig. 2(d)], in which Na1 sites order in rows parallel to the $\boldsymbol{a}_1+2\boldsymbol{a}_2$ direction with single or double Na2 rows interdispersed; the "large zigzag" pattern for $x=0.67$ [=4/6, Fig. 2(e)] and 0.71 [=5/7, Fig. 2(f)], where Na1 sites form a zigzag pattern with distance $2|\boldsymbol{a}_1|$ between nearest Na1 sites; and the "droplet" pattern for $x=0.77$ [=10/13, Fig. 2(g)], 0.81 [=13/16, Fig. 2(h)], 0.84 [=16/19, Fig. 2(i)], and 0.86 [=18/21, Fig. 2(j)], where three Na1 form droplet motifs. A justification for why these patterns occur is given in our previous work.[18]

2. Cluster expansion

Figure 3 shows the clusters included in the GGA cluster expansion. In-plane pair clusters that only contribute to the background are not shown. The circles at the intersections of the lines correspond to Na1 sites, and the circles inside the triangles represent Na2 sites. In one Na layer, Na2 sites are either all at the center of up-pointing triangles or all at the center of down-pointing triangles. These two occupancy patterns alternate as a result of $P2$ stacking. Circles in black correspond to sites in one layer, and circles in gray represent sites in an adjacent layer. The weighted CV score of this cluster expansion was 4.37 meV/f.u. The root mean square (rms) error was 3.29 meV/f.u. Within the set of structures calculated by first-principles, in-plane ordering of the cluster expansion ground-state structures matches the ordering of the first-principles ground states.

Figure 4 shows the total ECI (including background) for the GGA cluster expansion. Although all clusters are not shown, the nonzero background shown as the curve in Fig. 4 is applied to in-plane pair clusters up to 18 Å (the Na1-Na1 NN distance is 2.93 Å). The background ECI used was $V'_{ij}=12[\mathrm{erfc}(0.095r_{ij})/0.095r_{ij}]$ (meV). We can clearly observe that both in-plane and out-of-plane interactions are repulsive and convex decayings, and that the out-of-plane interactions decay much faster than the in-plane interactions. Our treatment of out-of-plane interactions as weaker—but not negligible—interactions compared to in-plane interactions is different from previous computational work, where electrostatic interactions out-of-plane and in-plane were not

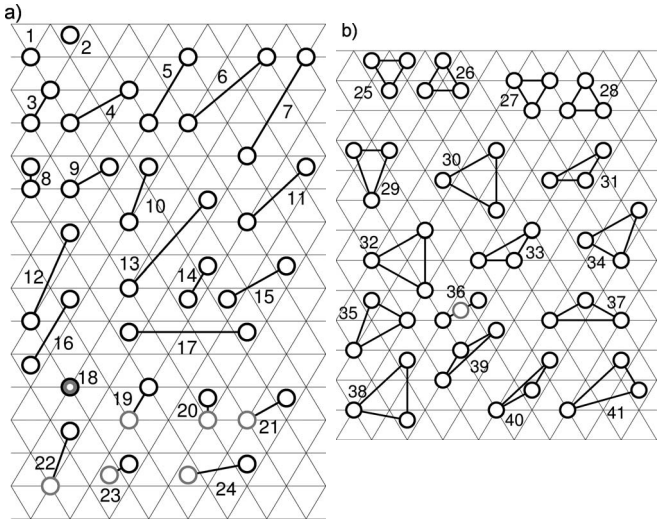

FIG. 3. Clusters with ECI different from the background included in the GGA cluster expansion. The circles at the intersections of the lines correspond to Na1 sites, and circles inside triangles represent Na2 sites. The circles in black correspond to sites in one layer, and the circles in gray represent sites in an adjacent layer. (a) Point and pair clusters. (b) Triplet clusters.

distinguished.[11,16] Furthermore, the magnitude of the pair interactions seems insensitive as to whether the sites in the pair are Na1 or Na2 sites. Table I shows the sum of the background ECIs and the fitted ECIs for clusters with nonzero value of the fitted ECIs. The cluster numbers in Table I correspond to the numbers in Fig. 3. The Na1-Na2 site energy difference $2(V^{\mathrm{Na1}}-V^{\mathrm{Na2}})$ from Table I is 61 meV/Na, which has the same magnitude compared to previous calculations (67 meV in Zhang *et al.*[16]).

The key interactions in Na_xCoO_2 were previously considered to be electrostatic in-plane[11,16] or short-range pair interactions.[15] Contrary to these speculations, in the GGA approximation we find that there are three different types of interactions, namely, strong long-range in-plane electrostatic interactions, strong relaxation effects, and weak short-range out-of-plane interactions. The in-plane screening mechanism is weak since they are less screened by the oxygen ions compared to out-of-plane interactions that extend over oxygen layers. In addition to electrostatic interactions, relaxation effects are necessary to accurately capture the energetics of the system; therefore, many triplet clusters had to be included in the cluster expansion. There is "empty space" between Na1 and patches of Na2 because simultaneous Na1-Na2 NN occupancy is not possible. Relaxation reduces this empty space in first-principles calculations. For example, in the ground-state structures for $x=0.67$, 0.71, and 0.76 [Figs. 2(e)–2(g)], the average relaxed Na1-Na2 second nearest-neighbor distance (corresponding to cluster 9 in Fig. 3) was consistently about 0.15 Å, or about 5% shorter than the distance on an ideal hexagonal lattice with the same cell volume. These relaxation effects can only be correctly captured by including triplets, or higher order clusters in the cluster expansion. The importance of capturing Na1-Na2 distances is shown by the fact that most significant triplets include a Na1-Na2 pair cluster as a subcluster [see Fig. 3(b)].

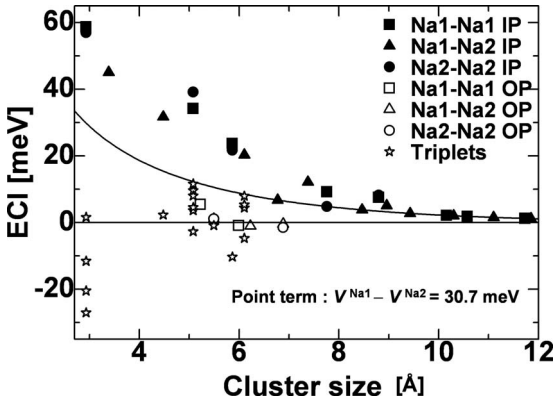

FIG. 4. Pair ECI for the GGA cluster expansion. Although all clusters are not shown, the nonzero background shown as the curve $V'_{ij}12\mathrm{erfc}(0.095r_{ij})/0.095r_{ij}$ is applied to in-plane pair clusters up to 18 Å (the Na1-Na1 NN cluster distance is 2.93 Å). The ECI shown are the sum of the background ECIs and the fitted ECIs. IP, in-plane and OP, out of plane.

3. Phase diagram

Figure 5 shows the phase diagram obtained with the GGA cluster expansion. The in-plane ordering of the ground states at $x=0.5$, 0.6, 0.67, 0.71, 0.77, and 0.81 are those shown in Fig. 2. Somewhat surprisingly, all the ordered phases are line compounds, tolerating very little off-stoichiometry. The phase-transition temperatures were obtained by free-energy integration. In the region $0.5<x<0.6$, Monte Carlo cooling simulations suggest short-range ordered structures with lower energy than the two-phase coexistence between known ordered patterns at $x=0.5$, 0.56 (5/9), and 0.6. One example of such a short-range ordered structure is shown in Fig. 6, a snapshot of a Monte Carlo cooling simulation at 100 K and $x\sim0.56$. We could not identify any regular pattern in these simulations. Upon heating the first-principles ground state at $x=0.56$, the energy monotonically increases until $T\sim230$ K, above which the energy decreases and the structure disorders. In principle, along an equilibrium path, the energy cannot decrease with temperature; thus, it gives further indication that a lower energy configuration must exist other than the one we identified. Detailed discussion of the short-range ordered structures is given later. For compositions $0.6\leq x\leq0.81$, the only ordered phase that persists to room temperature (300 K) is at $x=0.67$. In the composition range $0.85<x<1$, ground states have six-Na1 droplet motifs[15,18] analogous to the three-Na1 droplet motifs in Fig. 2. These six-Na1 droplet motifs are predicted to be ground states in the cluster expansion; however, we were unable to obtain a structure with six-Na1 droplet motifs as a ground state in first-principles calculations, possibly due to the fact that the optimum stacking of the in-plane ordered Na layers along the c_{hex} axis was not identified. The transition temperatures shown as dotted lines in the phase diagram in Fig. 5 are a lower bound.

Figure 7(a) shows the Na concentration, Na1/Na2 ratio, and Na1 order parameter in a Monte Carlo simulation where the system is heated at fixed chemical potential corresponding to $x\sim0.5$. The Na concentration does not change much

TABLE I. ECIs per meV in the cluster expansion for the GGA.

Points					
Cluster			ECI		
1			939.65		
2			908.94		
Pairs (excluding clusters with background contribution only)					
Na1-Na1		Na1-Na2		Na2-Na2	
Cluster	ECI	Cluster	ECI	Cluster	ECI
3	58.72	8	250.00	14	56.99
4	34.20	9	45.09	15	39.15
5	23.73	10	31.72	16	21.75
6	9.21	11	20.31	17	8.25
7	7.56	12	2.16		
		13	5.09		
18	5.45	20	1.03	23	1.12
19	−0.88	21	−1.03	24	−1.46
		22	−0.43		
Triplets					
Cluster	ECI	Cluster	ECI	Cluster	ECI
25	−20.48	31	−2.67	37	−10.31
26	−11.56	32	11.60	38	5.35
27	−11.56	33	3.63	39	4.41
28	−27.02	34	4.56	40	−4.69
29	2.32	35	8.04	41	7.94
30	9.59	36	−0.89		

with temperature; however, the Na1/Na2 ratio drops sharply at around 300 K. The order parameter is a measure of disorder and is 1 when fully ordered and 0 when fully disordered. For $Na_{0.5}CoO_2$, Na1 sites are split into α and β sites. Figure 2(b) shows the positions of α and β sites. Na1 [large gray circles in Fig. 2(b)] may occupy α sites but not β sites at 0 K. Defining the concentration of Na1 on α and β sites as c_α and c_β, respectively, the concentration of Na1 on α sites in the fully ordered state is $c_{\alpha 0}=0.5$, and the concentration of Na1 on β sites in the fully ordered state is $c_{\beta 0}=0$, the order parameter is given by

$$\frac{c_\alpha - c_\beta}{c_{\alpha 0} - c_{\beta 0}} = 2(c_\alpha - c_\beta). \tag{6}$$

In Fig. 7(a), the order parameter drops from approximately 1 to around 0 at about 300 K, exactly where the change in Na1/Na2 ratio is observed. Figure 7(b) shows a snapshot of a Na layer at 320 K. It is clear that the Na arrangement is disordered at this temperature.

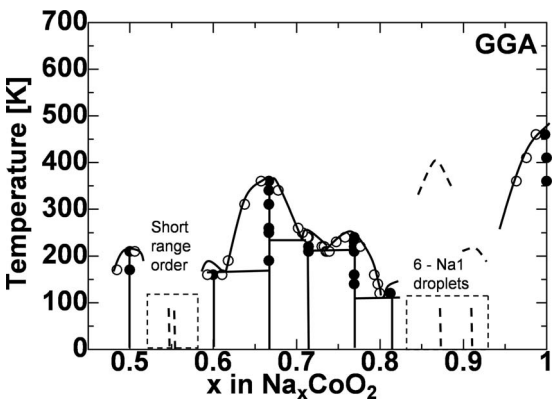

FIG. 5. GGA phase diagram obtained by Monte Carlo simulation from the cluster expansion in Table I.

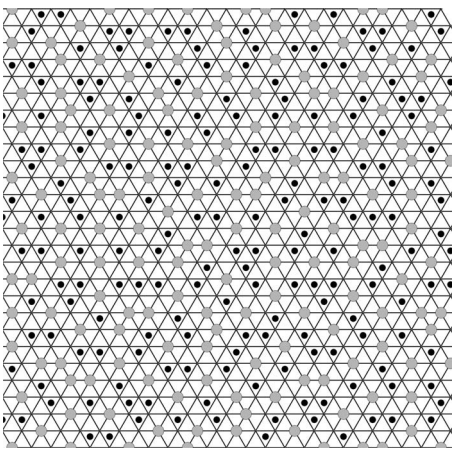

FIG. 6. Snapshot of a Na layer in a Monte Carlo cooling simulation at 100 K, concentration $x \sim 0.56$, GGA approximation. Legend: gray circles, Na1 and black circles, Na2.

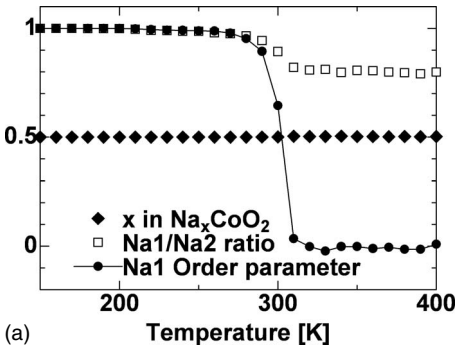

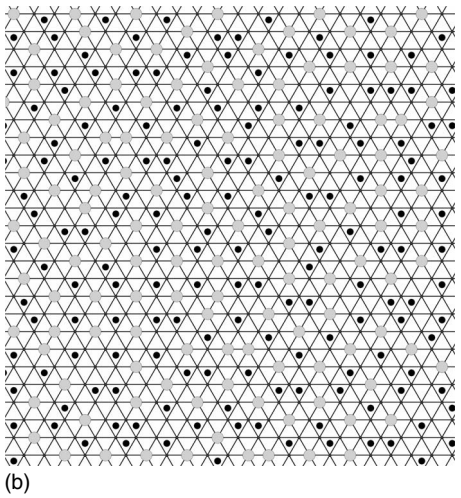

FIG. 7. (a) Na concentration, Na1/Na2 ratio, and Na1 order parameter for a Monte Carlo heating simulation near $x=0.5$ (GGA approximation). (b) Snapshot of a Monte Carlo cell at 320 K after transition. Legend: gray circles, Na1 and black circles, Na2.

The order-disorder temperature in the heating simulation of Fig. 7(a) is approximately 300 K, higher than the 220 K shown in the phase diagram in Fig. 5. This difference reflects the strong first-order character of the transition. In Monte Carlo simulations, phase transitions require that intermediate states between old and new states are accessible. If the energy levels of the intermediate states are high, increased temperature is necessary to bring the system from the metastable state to the stable state. In perfectly ordered states at higher Na concentrations, such as above $x \geq 0.5$, there are no low-energy excitations accessible to bring the system to the disordered state. As long as the ordering is perfect, there are no sites where Na can be added because simultaneous Na1-Na2 NN occupancy is prohibited. The system can disorder only by first making space through annihilating some Na, and then filling back the space by adding Na. The high energy required to overcome this excitation step is feasible only at elevated temperatures compared to the true transition temperature.

To obtain a sense of the reliability of the computed transition temperatures, the change in phase-transition temperature when the formation energy of the ground state is shifted by 1 meV/f.u. is calculated. This energy is added and/or subtracted to the ground-state energy but no change is made to the ECI. As a result, a lower and/or higher transition entropy is required at the transition. The extent of change can characterize the effect of inaccuracy in the cluster expansion on the phase-transition temperature. The sensitivity or change in phase-transition temperature with +1 meV shift in ground-state energy $\Delta T_c/\Delta E_{\text{shift}}$ for key phases was for $x=0.5$, −70 K; $x=0.67$, −40 K; $x=0.77$, −40 K; and $x=0.87$ (six-Na1 droplet), −70 K. In general, transition temperatures are more reliable for high transition temperatures since the free energy drops more steeply with change in temperature. However, the transition temperature for six-Na1 droplet phases are less reliable compared to those of $x \sim 0.67$ and 0.77.

Note that if the ordered structures are line compounds, then the shift in transition temperature can be estimated from the entropy of the disordered state,

$$\Delta T_c = \Delta E_{\text{shift}}/S_{\text{disorder}}. \tag{7}$$

The large shift ΔT_c in the transition temperature T_c with a small shift in formation energy ΔE_{shift} implies small entropies in the disordered states. One reason is that the restriction of Na1-Na2 NN simultaneous occupancy severely limits the number of possible Na ordering patterns; therefore, the Na layer is not totally disordered, and the entropy of the "disorder" phase is decreased.

B. GGA+U

1. Formation energies and ground states

Figure 8(a) shows the GGA+U formation energy per f.u. In contrast to the GGA result, the number of ground states is very small (five including the two end members) in the GGA+U approximation, although calculations have been conducted at 14 concentrations. The dotted line in Fig. 8(a) shows the convex hull when $O3$-$NaCoO_2$ (shown with the gray diamond) is considered as an end member. The GGA+U energy of $O3$-$NaCoO_2$ is 44 meV/f.u. lower than that of $P2$-$NaCoO_2$.

Figures 8(b)–8(e) shows the ground-state structures at $x=0.5$ [=2/4, Fig. 8(b)], 0.6 [=3/5, Fig. 8(c)], 0.67 [=4/6, Fig. 8(d)], and 0.75 [=9/12, Fig. 8(e)]. The Na layer ordering patterns for $x=0.5$ and 0.67 is the same as these in the GGA calculations; however, at $x=0.75$ the droplet ordering found in GGA+U is not a ground state in GGA. For each ground state, the stacking in the c-axis direction is such that Na1 between adjacent layers are positioned as far away from each other as possible and Co^{4+} stack on top of each other.

Strong ground states occur only at concentrations where the Co ordering pattern is commensurate with the symmetry of the Na lattice.[18] At $x=0.5$, 0.67, and 0.75, Co orders with a supercell of $a_{\text{hex}} \times \sqrt{3}a_{\text{hex}}$, $\sqrt{3}a_{\text{hex}} \times \sqrt{3}a_{\text{hex}}$, and $2a_{\text{hex}} \times 2a_{\text{hex}}$, respectively. The Na layer ordering for these structures is $2a_{\text{hex}} \times \sqrt{3}a_{\text{hex}}$, $2\sqrt{3}a_{\text{hex}} \times 2\sqrt{3}a_{\text{hex}}$, and $2\sqrt{3}a_{\text{hex}} \times 2\sqrt{3}a_{\text{hex}}$, respectively.

2. Cluster expansion

Figure 9 shows the clusters included in the GGA+U cluster expansion. As in the GGA, the empty circles at the intersections of the lines correspond to Na1 sites, and empty circles inside triangles represent Na2 sites. The filled circles

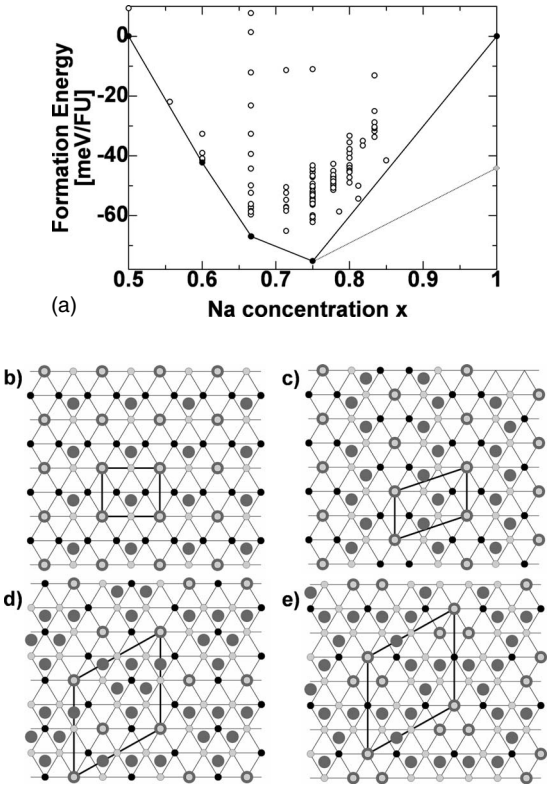

FIG. 8. (a) First-principles GGA+U formation energy per formula unit. The bold solid line shows the convex hull. The convex hull changes to the dotted line when formation of $O3$-$NaCoO_2$ (gray diamond) is allowed. [(b)-(e)] Ground states of first-principles GGA+U formation energy at x=(b) 0.5, (c) 0.6, (d) 0.67 (2/3), and (e) 0.75. Legend: large dark gray circles, Na; small light gray circles, Co^{3+}; and small black circles, Co^{4+}. Na1 sites are small light gray circles superimposed on dark gray circles.

correspond to Co sites. The weighted CV score of this cluster expansion was 9.33 meV/f.u., and the rms error was 3.12 meV/f.u. Within the structures calculated by first principles, in-plane ordering of cluster expansion ground-state structures matches the ordering of first-principles ground states. Figure 10 shows the ECI for the GGA+U cluster expansion. The Na-Co ECI has been multiplied by −1 to show interactions between more electrostatically repulsive species with a positive value. The Na1-Na2 NN and Na1-Co^{4+} NN simultaneous occupancy penalties have been added in the ECI. The Co NN pair is the strongest interaction, being almost four times higher in magnitude than the second strongest pair interaction. For this reason, strong ground states in Fig. 8 all have a well-ordered Co^{3+}/Co^{4+} layer (x=0.67 with $\sqrt{3}a_{hex} \times \sqrt{3}a_{hex}$ ordering and x=0.75 with $2a_{hex} \times 2a_{hex}$ ordering). The values of the ECI are shown in Table II. The cluster numbers in Table II correspond to the numbers in Fig. 9. Contrary to the GGA, insight on the Na1 and Na2 site energy difference cannot be obtained from the ECI in Table II since the magnitude of the Na1-Co^{4+} NN penalty affects the Na2 point term ECI. It could be argued that the Co interactions are too strongly represented in the cluster expansion, as a consequence of a too large value of U. U=5 eV/Co gives the right average electrochemical potential between $0.5 \leq x \leq 0.8$ [8] (details in Sec. IV); however, it may not be the optimum value of U to model partial charge localization, which is often observed in this material. However, our phase diagram results can be taken as a representation of the extreme scenario of complete charge localization.

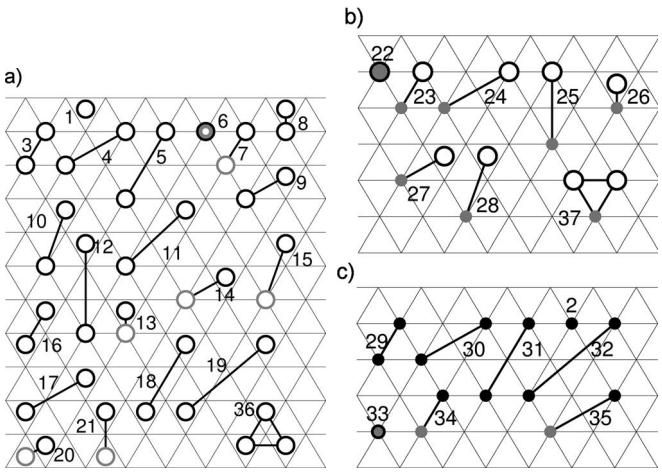

FIG. 9. Clusters included in the GGA+U cluster expansion. (a) Clusters of Na layer sites. (b) Clusters including both Na layer and Co layer sites. (c) Clusters of Co layer sites. The empty circles at the intersections of the lines correspond to Na1 sites, and the empty circles inside triangles represent Na2 sites. The filled circles correspond to Co sites. The circles in black correspond to sites in one layer, and the circles in gray represent sites in an adjacent layer.

3. Phase diagram

Figure 11 shows the phase diagram obtained with the GGA+U cluster expansion. The ground states at x=0.5, 0.67 (2/3), and 0.75 are shown in Figs. 8(b), 8(d), and 8(e), respectively. The order-disorder temperatures are typically higher than those in the GGA phase diagram, and the three ordered states are all stable at room temperature. In the region $0.5 < x < 0.67$, our Monte Carlo simulations again suggest structures with short-range order that have lower energy than phase coexistence between known ordered patterns at x=0.5, 0.6, and 0.67. Similar to the short-range order region in the GGA result, we could not identify any regular ordering

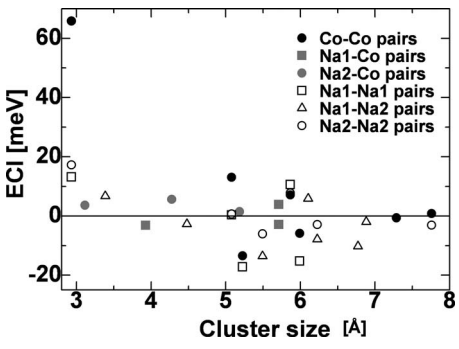

FIG. 10. Pair and triplet ECI for the GGA+U cluster expansion. The Na-Co ECI have been multiplied by −1 to show interactions between more electrostatically repulsive species with a positive value.

TABLE II. ECIs per meV for the cluster expansion in the GGA+U.

Points					
Cluster	ECI				
1	−154.40				
2	324.55				
Pairs					
Na1-Na1		Na1-Na2		Na2-Na2	
Cluster	ECI	Cluster	ECI	Cluster	ECI
3	13.17	8	250.00	16	17.28
4	0.36	9	6.73	17	0.65
5	10.60	10	−2.70	18	7.77
6	−17.19	11	5.88	19	−3.08
7	−15.24	12	−10.23	20	−6.04
		13	−13.58	21	−2.89
		14	−7.87		
		15	−1.96		
Pairs					
Na1-Co		Na2-Co		Co-Co	
Cluster	ECI	Cluster	ECI	Cluster	ECI
22	−100.00	26	−3.64	29	65.86
23	3.17	27	−5.64	30	13.09
24	2.89	28	−1.48	31	7.11
25	−3.89			32	0.82
				33	−13.42
				34	−5.88
				35	−0.62
Triplets					
Cluster	ECI				
36	−18.98				
37	−2.64				

patterns at zero Kelvin. At $x=0.67$, there are two order-disorder transitions. The Na layer initially disorders at approximately 370 K, followed by charge disorder in the Co layer at about 670 K. Contrary to the GGA phase diagram in Fig. 5, the six-Na1 droplet patterns are not stable in GGA+U since there is no high-symmetry Co^{3+}/Co^{4+} ordering pattern commensurate with the six-Na1 droplet pattern. Instead, there is a strong eutectic where the disordered phase is stable down to ~30 K near $x\sim0.86$.

IV. DISCUSSION

A. Generalized gradient approximation phase diagram

In the GGA we find ground-state structures at $x=0.5$, 0.6, 0.67, 0.71, 0.77, and 0.81. In addition, our Monte Carlo simulations indicate that other structures are likely to be present around $x=0.56$ though we could not identify these structures. While we do not report details here about the stacking sequence, we find that, in general, the lowest energy stacking is the one with the minimum amount of short adjacent-plane Na1-Na1 neighbors. Stacking often reduces the symmetry of the unit cell. For example, in the $Na_{0.67}CoO_2$ ground-state structure and structures with three-Na1 droplet motifs, stacking destroys the in-plane threefold rotation symmetry. However, in stronger ground states such as $Na_{0.50}CoO_2$ and $Na_{0.67}CoO_2$, mirror symmetry is retained.

Comparing calculated ground states with experimental information, we can provide the following information: Clear

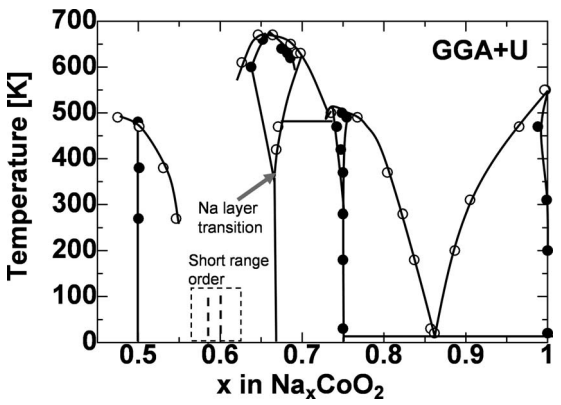

FIG. 11. GGA+U phase diagram obtained by Monte Carlo simulation from the cluster expansion in Table II.

TABLE III. The Warren–Cowley short-range order parameters (Ref. 67) for competing phases at $x \sim 0.56$. The Warren–Cowley parameter is >0 when the Na and vacancies have a phase separating tendency, <0 when there is a phase separating tendency, and 0 when fully random. NN, nearest-neighbor bond; FPGS, first-principles ground state; SRO, short-range order structure; and DIS, disordered structure.

Bond type	Na1-Na1 NN	Na2-Na2 NN	Na1-Na1 second NN	Na2-Na2 second NN	Na1-Na1 third NN	Na2-Na2 third NN
FPGS	−0.286	−0.167	0.143	0.000	−0.071	−0.167
SRO	−0.216	−0.172	0.000	−0.121	0.003	0.038
DIS	−0.130	−0.113	−0.028	−0.082	−0.035	−0.036

evidence exists for the presence of a stable ordered state at $x=0.5$ both experimentally[6,9] and from computational suggestions.[15,16] Experimentally, a structural transition at $x=0.5$ is observed at 210 K,[27] which is close to our GGA transition temperature at 220 K.

At $x=0.56$, no superstructure is observed in low-temperature electron diffraction by Zandbergen *et al.*;[12] however, a few crystals show the diffraction pattern common for the $x=0.5$ compound.[12] This is in fair agreement with our calculations, where short-range disorder is seen. To understand the origin of the structures observed in the Monte Carlo cooling simulation at $0.5<x<0.6$, the Warren–Cowley short-range order parameters[67] of the three shortest Na1-Na1 and Na2-Na2 bonds were calculated and summarized in Table III for the $x=0.56$ first-principles ground state [Fig. 2(c)], a short-range ordered structure from Monte Carlo simulation (Fig. 6, $T=100$ K), and a disordered structure from Monte Carlo simulation ($T=650$ K). The Warren–Cowley parameter α_n is defined for the nth nearest neighbor on a binary sublattice with species A and B as $\alpha_n=1-p_{AB}^n/p_{AB}^{\text{rand}}$. In this work, Warren–Cowley parameters are calculated on either the Na1 and/or vacancy or the Na2 and/or vacancy sublattice, and the two species A and B are chosen as Na1 and vacancies in the Na1 sublattice, or Na2 and vacancies in the Na2 sublattice. Here, p_{AB}^n is the probability of A-B (Na1-vacancy or Na2-vacancy in this work) pairs with nth nearest-neighbor distance in the system in consideration, and $p_{AB}^{\text{rand}}=c_A c_B$ is the probability of A-B pairs if A and B were randomly distributed.[68] The Warren–Cowley parameter is >0 when the two species have an ordering tendency, <0 when the species have a phase separating tendency, and 0 when fully random. In this paper, the two species are chosen as Na1 and vacancies in the Na1 sublattice, or Na2 and vacancies in the Na2 sublattice.

It is clear from these Warren–Cowley parameters that the Monte Carlo simulation at 100 K is not simply in a state between the ordered ground state and the random solution. While the NN Na1-Na1 Warren–Cowley parameter indicates lower order than the ground state, the NN and second NN Na2-Na2 Warren–Cowley parameters indicate stronger ordering than in the ground state. This would indicate that there might be a lower energy ground state possible. The ground state for $x=0.6$ is the state predicted by previous computational work.[15,16] However, this ground state has not been observed experimentally.

The electron-diffraction results by Zandbergen *et al.*[12] for $Na_{0.64}CoO_2$ show no superstructure. This does not contradict our result. At that composition and room temperature, our phase diagram (Fig. 5) shows a two-phase region with mostly a disordered phase and possibly a small amount of $x=0.67$ compound, depending on the exact composition of the phase boundaries and the sample. Our calculations find new ground states at 0.67 (2/3) and 0.714 (5/7). These ground states have a larger unit cell than speculated in previous computational work;[15,16] therefore, the ground-state ordering pattern may have been overlooked in that work. We are not aware of experimental papers suggesting our ground-state ordering patterns. Chou *et al.*[69] suggested a ground state at $x=0.708$ (17/24) with $2\sqrt{3}a_{\text{hex}}\times 2\sqrt{3}a_{\text{hex}}$ ordering that has 3-Na1 droplet motifs with trivacancies (Na concentration $x=9/12$) in half of the layers and 3-Na1 droplet motifs with quadrivacancies (Na concentration $x=8/12$) in the other half of the layers. However, the GGA energy of that structure is 15 meV/f.u. higher than two-phase coexistence of our $x=0.67$ and 0.714 ground states.

Contrary to previous computational work,[15,16] no ground state is observed in the GGA approximation at $x=0.75$, and the lowest-energy state at this composition is two-phase coexistence between $x=0.71$ and 0.77. This is in excellent agreement with neutron-diffraction results on powdered crystals by Huang *et al.*[9] Electron diffraction at low temperature by Zandbergen *et al.*[12] suggests a complicated and weak superstructure at $x=0.75$, and during experiment, the superstructure pattern was quickly modified by the electron beam. Therefore, it is plausible that no stable ordering patterns exist at $x=0.75$. Experimentally, using resistivity measurements two transitions are observed for the $x=0.75$ system at around 285 and 315 K.[11] In the GGA phase diagram, we also see two transitions at this Na concentration: a eutectic transition around 200 K and an order-disorder transition around 230 K. While our calculated temperatures are lower than what is observed, the temperature difference between the two transitions is strikingly similar. Hence, our simulation results may explain these transitions as two consecutive first-order transitions toward the disordered state.

At the high concentration end we find the droplet phases first suggested by Roger *et al.*[11] and also identified in previous computational work.[15,18] Six-Na1 droplets, although suggested computationally as ground states,[15,18] have not been observed experimentally. However, in our first-principles calculations we were not able to find a structure with six-Na1 droplets that was stable compared to phase separation between the three-Na1 droplet phase with $P2$ stacking at $x=0.86$ and $P2$-$NaCoO_2$. Furthermore, if two phase formation between $P2$ three-Na1 droplet phase and $O3$-$NaCoO_2$ is allowed, the six-Na1 droplet motifs would become metastable with regard to this two-phase formation. Although at first glance ground states for the three-Na1 motifs seem to appear

at random compositions, in fact such ground states appear only at compositions $x=(N-3)/N$, where N is an integer and the unit cell has $\sqrt{N}a_{\mathrm{hex}}\times\sqrt{N}a_{\mathrm{hex}}$ ordering in plane. The only exception is $x=13/16$, where the structure with $4a_{\mathrm{hex}}\times 4a_{\mathrm{hex}}$ ordering has 1.6 meV/f.u. higher energy than the ground state with $4a_{\mathrm{hex}}\times\sqrt{13}a_{\mathrm{hex}}$ ordering. This fact implies that in principle three-Na1 droplet motifs want to spread apart as far away as possible from each other without destroying threefold rotation symmetry in plane. It is possible that more ground states with 3-Na1 motifs may exist, and the four ground states shown in Figs. 2(g)–2(j) are part of an infinite series of ground states with $\sqrt{N}a_{\mathrm{hex}}\times\sqrt{N}a_{\mathrm{hex}}$ ordering in-plane. The stacking in the c-axis direction is such that Na1 between adjacent layers are positioned as far away from each other as possible.

B. GGA+U phase diagram

In the GGA+U approximation, we find ground-state structures at $x=0.5$, 0.67, and 0.75. Furthermore, our Monte Carlo simulations indicate that other structures are likely present around $x=0.60$, although we could not identify these structures. The Na layer ordering patterns of $x=0.5$ and 0.67 ground states are the same as in the GGA phase diagram. The 0.75 ground state, with three-Na1 droplet motifs, is the ordering proposed by Roger *et al.*[11] and did not appear in the GGA phase diagram. Figure 12 shows a snapshot of the Na layer of a Monte Carlo cooling simulation at 430 K and composition $x\sim 0.76$. Besides the $x=0.75$ ground-state patterns, we are also able to observe connected three-Na1 droplet motifs, and in one region the connected three-Na1 droplet motifs and Na2 show the "stripe" pattern proposed by Geck *et al.*[13] based on observations with high-energy XRD near $x=0.75$. This concentration range is exactly where partial charge localization is experimentally observed.[21–24]

In the GGA+U approximation, complete charge localization to Co^{3+} and Co^{4+} occurs, and the dominating interactions are interactions between Co. Furthermore, ground states must have stable Na layer ordering that is commensurate with the Co layer ordering and such that there is no Na1-Co^{4+} NN simultaneous occupancy. For these reasons, there are very few stable ordered structures in the GGA+U phase diagram. Only partial charge localization has been observed experimentally. Therefore, interactions between Co are expected to be weaker than in the GGA+U approximation. Weaker interactions would allow for more Co layer disorder at lower temperature, and real Co layer order-disorder transition temperatures should be lower compared to those in the phase diagram. In fact, the transition temperature at $x=0.75$ is much overestimated compared to measurements by Roger *et al.*[11]

C. Comparison of generalized gradient approximation and GGA+U

1. Interactions

The GGA and GGA+U phase diagrams are considerably different. Only at $x=0.5$ and $x=0.67$ do they give the same ground states. The transition temperatures in the GGA+U phase diagram are considerably higher than in the GGA diagram. This difference between the two electronic structure approximations should not be surprising. In GGA the mixed valence on Co is metallic and delocalized so that only interactions between Na^+ exist. The Na^+-Na^+ repulsion is strongly screened by the charge in the hybridized Co-O orbitals leading to weak effective interactions and low order-disorder transition temperatures. This situation is reminiscent of the related compound Li_xCoO_2, in which similar strong screening of the Li^+ ion by a Co-O rehybridization[48,70,71] also leads to rather low order-disorder transition temperatures.[32]

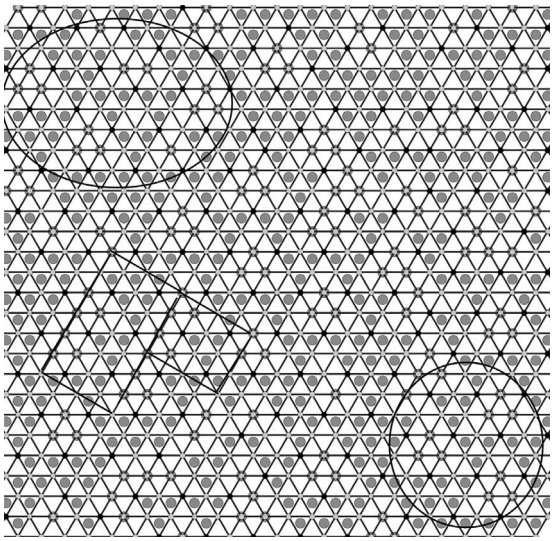

FIG. 12. Snapshot of a Monte Carlo cooling simulation at 430 K, concentration $x\sim 0.76$, GGA+U approximation. The "stripe" motif proposed by Geck *et al.* (Ref. 13) (shown in rectangles) and the ground-state motif for $x=0.75$ (circled) are visible. Legend: large dark gray circles, Na; small light gray circles, Co^{3+}; and small black circles, Co^{4+}. Na1 sites are small light gray circles superimposed on dark gray circles.

Application of the GGA+U leads to completely different physics. The value of U is strong enough to cause charge localization and the phase diagram is largely governed by the strong Co^{3+}/Co^{4+} interaction. The Co^{3+}-Co^{4+} effective interaction is much stronger than the Na^+-vacancy one, a fact that results in maximal separation of Co^{4+} in the ground states shown in Figs. 8(b)–8(e). In addition GGA+U further imposes the constraint that Na1 and Co^{4+} cannot be adjacent. Therefore, there are restrictions on how the Na layers and Co layers can stack. Strong ground states, namely, at $x=0.5$, 0.67, and 0.75, retain mirror symmetry perpendicular to the oxygen layers. To retain mirror symmetry at a composition such as $x=0.6$, Na1 have to stack on top of each other, which is energetically unfavorable and hence there is no ground state.

When two ordered states on different sublattices are coupled they can either go through separate or through a single order-disorder transition. This depends mainly on the symmetry relation between the two sublattices.[62] In the ground-state structure at $x=0.67$ Co-charge ordering does not break the symmetry on the Na2 sublattice but reduces the number of available Na1 sites. In this case we see a distinct

Na disorder transition before the Co-charge state disorders. The Na disorder transition temperature at $x=0.67$ is almost the same ($T\sim 370$ K) as in the GGA, indicating that both descriptions are somewhat consistent for the Na configurational energy. At all other compositions the Na-vacancy and Co^{3+}/Co^{4+} sublattices disorder simultaneously, reflecting the fact that the Na ordering is determined by the symmetry breaking arising from the charge ordering on the Co sublattice.

It is important to understand the limitations of the GGA $+U$ cluster expansion and Monte Carlo simulation at elevated temperature. The Co^{4+} is fully localized and therefore contributes significant configurational-like electronic entropy to the system in our model. If the electronic hole were to delocalize—as in a metal-insulator transition—this description would become invalid, and a metallic Fermi–Dirac-type entropy would be more appropriate.

2. Comparison to experimental Na potential, lattice parameter, and Na1/Na2 ratio

To further assess the merits of the GGA and GGA$+U$ methods to this system, we also compare the Na intercalation voltage, c lattice parameter, and Na1/Na2 ratio from our Monte Carlo simulation results with experimental observations.

a. Na potential. Electrochemical cells can be constructed with a Na_xCoO_2 electrode to remove Na in a controlled manner.[8,10] The measured voltage as a function of concentration represents the Na chemical potential in the material and can accurately show the concentration at which stable phases exist and their relative energy differences. Plateaus in the voltage curve indicate two-phase regions. Figure 13(a) shows the Na intercalation and/or deintercalation voltage for GGA and GGA$+U$ at 200 and 300 K as a function of Na concentration. The computed voltage is the difference between the Na chemical potential at the cathode (Na_xCoO_2) and anode (pure Na) and can be obtained directly from the Monte Carlo simulations. The shape of the GGA and GGA $+U$ voltage curves are very different, reflecting the different physics in the two approximations. Above $x>0.8$ we were not able to point out the exact compositions of the ground states in the GGA; therefore, an accurate voltage curve cannot be obtained in this composition range. The GGA voltage curve has a larger average voltage drop between $x=0.5$ and 0.8. In GGA$+U$, there is a very stable phase at $x=0.75$, which is not seen in GGA. Stable phases are observed at $x=0.71$ and $x=0.77$ in the GGA voltage curve at 200 K, but these features are lost in the GGA 300 K voltage curve.

Matching and comparing the experimental and computed voltage curves requires several adjustments. From work on the related Li materials, it is well known that in GGA the redox potential can be underestimated by 0.5 to 1 V (Ref. 53) due to the spurious self-interaction that the electron sees in the 3d orbital of Co. In addition, while electrochemical measurements are highly accurate at measuring relative changes in Na content, often the starting stoichiometry of the compound is in doubt due to the volatility of Na during synthesis.[29,30] Hence, in Fig. 13(b) we mainly compare the

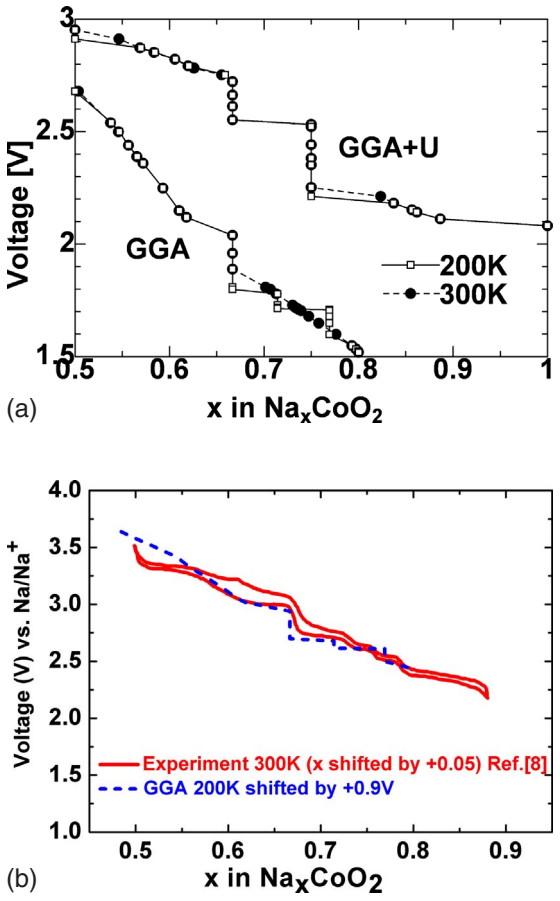

FIG. 13. (Color online) (a) Na intercalation/deintercalation voltage of Na_xCoO_2 when used as a cathode against pure Na anode which is derived from Monte Carlo simulations in the GGA and the GGA$+U$ at 200 and 300 K. (b) Comparison of experimental electrochemical voltage measurements from Delmas *et al.* (Ref. 8) at room temperature (red/gray bold line) with GGA 200 K voltage curve (blue/gray dotted line). The concentration of the experimental curve is shifted by +0.05, and the voltage of the GGA 200 K curve is shifted by +0.9 V.

shape of the computed and experimentally measured voltage curve. The experimental data are from electrochemical measurements at room temperature by Delmas *et al.*[8] The computational data are the GGA voltage curve at 200 K, with the voltage shifted upwards by 0.9 V. Out of the voltage curves in Fig. 13(a), the GGA 200 K curve shown in Fig. 13(b) most closely matches the experimental curve in these three aspects: (1) magnitude of the voltage drop (~1 V) between $x=0.5$ and $x=0.8$, (2) magnitude of the stable voltage region at $x\sim 0.67$, and (3) the existence of several stable phases at $x\sim 0.71$ and 0.77.

Since the stable phases at $0.7<x<0.8$ do not exist in the GGA 300 K voltage curve, it is possible that in this region GGA underestimates the transition temperatures. Previous computational phase diagrams based on GGA approximations in Li_xCoO_2 (Ref. 32) and Li_xNiO_2 (Ref. 33) have overpredicted phase-transition temperatures. The overestimation is speculated not to be due to intrinsic errors of the GGA approximation but rather to considering too few interactions

in the Li_xCoO_2 (Ref. 32) and Li_xNiO_2 (Ref. 33) cluster expansions, and as a result, some short-range interactions were overestimated. An alternate possibility is that no direct Na-Co coupling was treated in the Na_xCoO_2 GGA cluster expansion. The Co-sublattice affects interactions on the Na sublattice in Na_xCoO_2, but in Li_xCoO_2 and Li_xNiO_2 there are weak or no effects on Li from the Co sublattice. Another possible explanation is that temporal Co-charge localization occurs in the real system and this is not captured in the GGA, causing errors in phase-transition temperatures. Experimental observation of Curie–Weiss behavior implies existence of some extent of charge localization.[10]

While the GGA+U voltage curves match the absolute average experimental voltage better than GGA, its shape does not reflect experimental information: The stable phases at $0.7<x<0.8$ observed experimentally are wiped out by the $x=0.75$ stable phase in GGA+U. The stability of the $x=0.75$ phase in GGA+U comes solely from the fact that the strength of Co^{3+}-Co^{4+} interactions is overestimated in GGA+U and leads to a very stable Co^{3+}/Co^{4+} ordering pattern at $x=0.75$.

Electrochemical methods by Shu *et al.*[10] suggest stable phases at $x=0.5$, 0.55, 0.71 and 0.75. Susceptibility measurements on samples with $x=0.55$ are clearly different from those with $x=0.5$, indicating that these two compositions may be distinct phases.[10] In the work of Shu *et al.*,[10] no stable (or very weak) phase is reported for $x=0.67$, which is contradictory to previous electrochemical measurements by Delmas *et al.*[8] that suggested a stable phase close to $x=0.67$.

b. c lattice parameter. The c lattice parameter is a good measure of Na concentration, as increased Na concentration decreases the spacing between adjacent oxygen layers and may be used as a simple method to estimate the Na composition based on diffraction data. Figure 14 compares the c lattice parameters of the ground states (Figs. 2 and 8) obtained from first-principles GGA and GGA+U calculations at 0 K against neutron powder-diffraction data of polycrystalline Na_xCoO_2 by Huang *et al.*[9] The c lattice parameters from polycrystalline and single-crystal samples differ slightly, and the GGA c lattice parameter well matches the experimental results for polycrystalline samples.[18] The GGA c lattice parameter is well fitted in a quadratic form as $c=11.79412-1.15505x-0.18785x^2$, where x is the Na concentration. In GGA+U the c lattice parameter is overestimated.

c. Na1/Na2 ratio. Compared to the c lattice parameter that varies smoothly with Na concentration, the Na1/Na2 ratio is a more detailed measure of the accuracy of our calculations since errors in the Na1 and Na2 site energy difference show up in the Na1/Na2 ratio but not necessarily in the c lattice parameter. Figure 15 compares the Na1/Na2 ratio from Monte Carlo simulations at 200 and 300 K in the GGA and at 200 K in the GGA+U to the values obtained from neutron diffraction.[9,11,14,72,73] The Na1/Na2 ratio for 200 K is shown since the GGA voltage curve for 200 K better matches the experimental voltage curve compared to the 300 K curve. In GGA+U, the Na1/Na2 ratio for 200 and 300 K almost overlaps, therefore the latter is not shown in Fig. 15. The measurements of Huang *et al.*[9] at $x\sim0.56$ and 0.63 are very close to the GGA simulation results at 200 K. Below $x<0.7$ the GGA results match the experimental Na1/Na2 ratio better; however, above $x>0.7$ neither approximation clearly matches the experimentally observed ratio.

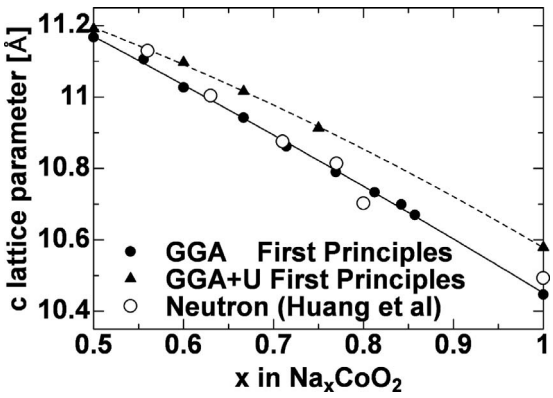

FIG. 14. c lattice parameter as a function of Na concentration computed from GGA and GGA+U first-principles calculations at 0 K and from neutron powder-diffraction results by Huang *et al.* (Ref. 9). The lines show a parabolic fit to the calculated c lattice-parameter values in the GGA and GGA+U approximations.

D. Additional discussion

At high Na concentrations, the Co^{4+} hole concentration is small and the holes are likely to be localized, leading to charge-density variation in the Co layer. Experimentally, slight charge localization is observed at $x=0.75$ [21–23] and $x=0.82$.[24] In this case, GGA+U may be a relevant approximation. However, even in this limit one cannot take the GGA+U results at face value since it is a static method and dynamic fluctuations may be needed to properly describe the electronic structure.[70] Furthermore, in the high composition range $x>0.82$, the thermodynamically stable state is two-

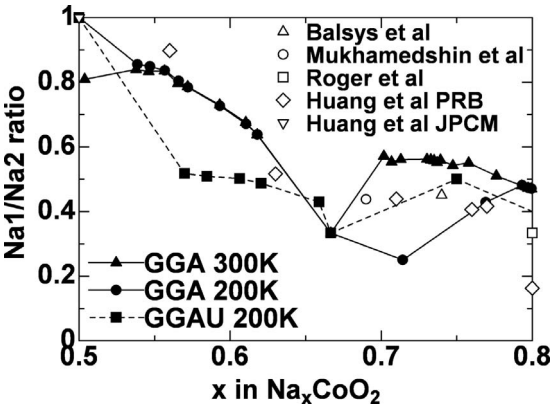

FIG. 15. Na1/Na2 ratio from Monte Carlo simulations at 200 and 300 K in GGA and 200 K in GGA+U approximations and from neutron-diffraction results (Refs. 9, 11, 14, 72, and 73). The filled symbols show computational results, and the open symbols represent experimental results.

phase separation into $P2$-Na_xCoO_2 and $O3$-$NaCoO_2$ (Figs. 2 and 8). Whether this occurs may depend on sample preparation and experimental conditions, further complicating a comparison between experiments and computation.

At lower Na concentrations ($x<0.8$), there are more holes in the Co layer of the system, and the hole concentration is well above the critical concentration at which a Mott transition to a metallic state can occur.[70] In the related system, Li_xCoO_2, this is indeed what occurs between $x=0.75$ and $x=0.95$.[4,70] As Na^+ is larger than Li^+ the Co-Co separation in Na_xCoO_2 is larger, and a complete transition to a metallic state may not occur because the orbital overlap between Co is reduced. This effect is more profound at higher Na concentration: The Co-Co distance is approximately 2.89 Å in $O3$-$NaCoO_2$ [74] and 2.81 Å in $O3$-$LiCoO_2$.[75] The Co-Co distance becomes shorter as the Na content is reduced, becoming approximately 2.81 Å in $P2$-$Na_{0.5}CoO_2$.[6] Even if the holes have tendency to localize, conductivity measurements indicate that they are mobile and can hop fairly quickly. As a result, when time averaged, the spatial distribution of holes would overlap, and the charge density becomes constant in the Co layer. Therefore, the GGA approximation may be appropriate at lower Na concentrations. Furthermore, the analysis of Na intercalation voltage, c lattice parameter, and ground states suggests that between $0.5\leq x\leq 0.8$, GGA is a better approximation than GGA+U.

It is important to note that in both GGA and GGA+U methods, it is impossible to observe metal-insulator transitions or a Curie–Weiss metal to spin-density wave metal transition,[19] if any occur. Furthermore, magnetic transitions cannot be observed in the phase diagrams since the spins on Co were only allowed to be ferromagnetically aligned in this work. Since GGA+U is a static method, partial Co-charge localization cannot be achieved for itinerant electrons. To incorporate the effects of partial charge localization, methods such as DMFT (Ref. 7) could be attempted but would be very computationally intensive for phase diagram constructions due to the large number of total energies required.

V. CONCLUSION

We successfully applied the cluster expansion technique and Monte Carlo simulations to obtain temperature-composition phase diagrams of $P2$-Na_xCoO_2 in both GGA and GGA+U approximations. The governing interactions between Na^+ are long-range electrostatics in-plane and relaxation effects in the GGA, and Co layer interactions dominate other interactions such as Na layer interactions in the GGA+U. There are at least ten ground states in the concentration range $0.5\leq x\leq 1$ including the two end members in the GGA compared to only five in the GGA+U. Most order-disorder transition temperatures for ground states are below room temperature in GGA, whereas transition temperatures of ground states are above room temperature in GGA+U. Comparison of Monte Carlo simulation results with experimental data, such as structural transition temperature, Na intercalation and/or deintercalation voltage, c lattice parameter, and Na1/Na2 ratio, consistently suggests that GGA is a better approximation in the composition range $0.5\leq x<0.8$. A cluster expansion formalism incorporating long-range electrostatic interactions was used.

ACKNOWLEDGMENTS

This work was supported by the Office of Basic Energy Sciences, U.S. Department of Energy under Contract No. DE-FG02-96ER-45571. We thank the National Partnership for Advanced Computational Infrastructure (NPACI) for computing time. Y.S.M. thanks A. Van der Ven and D. Carlier for fruitful discussion. Y.H. thanks T. Mueller and A. Van der Ven for the cluster expansion and Monte Carlo simulation codes. We also thank C. Delmas for generously providing data from electrochemical experiments.

*gceder@mit.edu

[1] I. Terasaki, Y. Sasago, and K. Uchinokura, Phys. Rev. B **56**, R12685 (1997).
[2] M. Lee, L. Viciu, L. Li, Y. Y. Wang, M. L. Foo, S. Watauchi, R. A. Pascal, R. J. Cava, and N. P. Ong, Nat. Mater. **5**, 537 (2006).
[3] K. Takada, H. Sakurai, E. Takayama-Muromachi, F. Izumi, R. A. Dilanian, and T. Sasaki, Nature (London) **422**, 53 (2003).
[4] M. Menetrier, I. Saadoune, S. Levasseur, and C. Delmas, J. Mater. Chem. **9**, 1135 (1999).
[5] C. Delmas, C. Fouassier, and P. Hagenmuller, Physica B & C **99**, 81 (1980).
[6] A. J. Williams, J. P. Attfield, M. L. Foo, L. Viciu, and R. J. Cava, Phys. Rev. B **73**, 134401 (2006).
[7] C. A. Marianetti and G. Kotliar, Phys. Rev. Lett. **98**, 176405 (2007).
[8] C. Delmas, J. J. Braconnier, C. Fouassier, and P. Hagenmuller, Solid State Ionics **3-4**, 165 (1981).
[9] Q. Huang, M. L. Foo, R. A. Pascal, J. W. Lynn, B. H. Toby, Tao He, H. W. Zandbergen, and R. J. Cava, Phys. Rev. B **70**, 184110 (2004).
[10] G. J. Shu, A. Prodi, S. Y. Chu, Y. S. Lee, H. S. Sheu, and F. C. Chou, Phys. Rev. B **76**, 184115 (2007).
[11] M. Roger, D. J. P. Morris, D. A. Tennant, M. J. Gutmann, J. P. Goff, J.-U. Hoffmann, R. Feyerherm, E. Dudzik, D. Prabhakaran, A. T. Boothroyd, N. Shannon, B. Lake, and P. P. Deen, Nature (London) **445**, 631 (2007).
[12] H. W. Zandbergen, M. Foo, Q. Xu, V. Kumar, and R. J. Cava, Phys. Rev. B **70**, 024101 (2004).
[13] J. Geck, M. v. Zimmermann, H. Berger, S. V. Borisenko, H. Eschrig, K. Koepernik, M. Knupfer, and B. Büchner, Phys. Rev. Lett. **97**, 106403 (2006).
[14] Q. Huang, M. L. Foo, J. W. Lynn, H. W. Zandbergen, G. Lawes, Yayu Wang, B. H. Toby, A. P. Ramirez, N. P. Ong, and R. J. Cava, J. Phys.: Condens. Matter **16**, 5803 (2004).
[15] Y. L. Wang and J. Ni, Phys. Rev. B **76**, 094101 (2007).
[16] P. H. Zhang, R. B. Capaz, M. L. Cohen, and S. G. Louie, Phys.

Rev. B **71**, 153102 (2005).
[17] Y. S. Meng, A. Van der Ven, M. K. Y. Chan, and G. Ceder, Phys. Rev. B **72**, 172103 (2005).
[18] Y. S. Meng, Y. Hinuma, and G. Ceder, J. Chem. Phys. **128**, 104708 (2008).
[19] M. L. Foo, Y. Y. Wang, S. Watauchi, H. W. Zandbergen, T. He, R. J. Cava, and N. P. Ong, Phys. Rev. Lett. **92**, 247001 (2004).
[20] M. Onoda and T. Ikeda, J. Phys.: Condens. Matter **19**, 186213 (2007).
[21] T. Motohashi, R. Ueda, E. Naujalis, T. Tojo, I. Terasaki, T. Atake, M. Karppinen, and H. Yamauchi, Phys. Rev. B **67**, 064406 (2003).
[22] J. Sugiyama, H. Itahara, J. H. Brewer, E. J. Ansaldo, T. Motohashi, M. Karppinen, and H. Yamauchi, Phys. Rev. B **67**, 214420 (2003).
[23] L. M. Helme, A. T. Boothroyd, R. Coldea, D. Prabhakaran, D. A. Tennant, A. Hiess, and J. Kulda, Phys. Rev. Lett. **94**, 157206 (2005).
[24] S. P. Bayrakci, I. Mirebeau, P. Bourges, Y. Sidis, M. Enderle, J. Mesot, D. P. Chen, C. T. Lin, and B. Keimer, Phys. Rev. Lett. **94**, 157205 (2005).
[25] D. J. Singh, Phys. Rev. B **61**, 13397 (2000).
[26] K.-W. Lee and W. E. Pickett, Phys. Rev. Lett. **96**, 096403 (2006).
[27] H. X. Yang, C. J. Nie, Y. G. Shi, H. C. Yu, S. Ding, Y. L. Liu, D. Wu, and N. L. Wang, Solid State Commun. **134**, 403 (2005).
[28] T. Motohashi, R. Ueda, E. Naujalis, T. Tojo, I. Terasaki, T. Atake, M. Karppinen, and H. Yamauchi, Physica B **329**, 914 (2003).
[29] F. C. Chou, E. T. Abel, J. H. Cho, and Y. S. Lee, J. Phys. Chem. Solids **66**, 155 (2005).
[30] J. Molenda, C. Delmas, P. Dordor, and A. Stoklosa, Solid State Ionics **12**, 473 (1984).
[31] F. C. Chou, J. H. Cho, and Y. S. Lee, Phys. Rev. B **70**, 144526 (2004).
[32] A. Van der Ven, M. K. Aydinol, G. Ceder, G. Kresse, and J. Hafner, Phys. Rev. B **58**, 2975 (1998).
[33] M. E. Arroyo y de Dompablo, A. Van der Ven, and G. Ceder, Phys. Rev. B **66**, 064112 (2002).
[34] A. Van der Ven and G. Ceder, Electrochem. Commun. **6**, 1045 (2004).
[35] Y. Hinuma, Y. S. Meng, K. Kang, and G. Ceder, Chem. Mater. **19**, 1790 (2007).
[36] F. Zhou, T. Maxisch, and G. Ceder, Phys. Rev. Lett. **97**, 155704 (2006).
[37] C. Wolverton and A. Zunger, Phys. Rev. B **57**, 2242 (1998).
[38] A. Van de Walle and M. Asta, Metall. Mater. Trans. A **33**, 735 (2002).
[39] J. M. Sanchez, F. Ducastelle, and D. Gratias, Physica A **128**, 334 (1984).
[40] D. de Fontaine, *Solid State Physics: Advances in Research and Applications* (Academic Press, San Diego, 1994), Vol. 47, p. 33.
[41] G. Ceder, A. Van der Ven, C. Marianetti, and D. Morgan, Modell. Simul. Mater. Sci. Eng. **8**, 311 (2000).
[42] M. Asta, S. M. Foiles, and A. A. Quong, Phys. Rev. B **57**, 11265 (1998).
[43] C. Wolverton, Philos. Mag. Lett. **79**, 683 (1999).
[44] V. Ozolins, B. Sadigh, and M. Asta, J. Phys.: Condens. Matter **17**, 2197 (2005).
[45] M. Asta, V. Ozolins, and C. Woodward, JOM **53**, 16 (2001).
[46] C. Wolverton and D. de Fontaine, Phys. Rev. B **49**, 8627 (1994).
[47] M. Asta, C. Wolverton, D. de Fontaine, and H. Dreyssé, Phys. Rev. B **44**, 4907 (1991).
[48] C. Wolverton and A. Zunger, Phys. Rev. Lett. **81**, 606 (1998).
[49] C. Wolverton and A. Zunger, J. Electrochem. Soc. **145**, 2424 (1998).
[50] P. E. Blochl, Phys. Rev. B **50**, 17953 (1994).
[51] G. Kresse and J. Furthmuller, Comput. Mater. Sci. **6**, 15 (1996).
[52] J. P. Perdew, K. Burke, and Y. Wang, Phys. Rev. B **54**, 16533 (1996).
[53] F. Zhou, M. Cococcioni, C. A. Marianetti, D. Morgan, and G. Ceder, Phys. Rev. B **70**, 235121 (2004).
[54] F. Zhou, C. A. Marianetti, M. Cococcioni, D. Morgan, and G. Ceder, Phys. Rev. B **69**, 201101(R) (2004).
[55] F. Zhou, K. Kang, T. Maxisch, and G. Ceder, Solid State Commun. **132**, 181 (2004).
[56] H. J. Kulik, M. Cococcioni, D. A. Scherlis, and N. Marzari, Phys. Rev. Lett. **97**, 103001 (2006).
[57] L. Wang, T. Maxisch, and G. Ceder, Phys. Rev. B **73**, 195107 (2006).
[58] K. W. Lee and W. E. Pickett, J. Appl. Phys. **99**, 08P702 (2006).
[59] A. I. Liechtenstein, V. I. Anisimov, and J. Zaanen, Phys. Rev. B **52**, R5467 (1995).
[60] S. L. Dudarev, G. A. Botton, S. Y. Savrasov, C. J. Humphreys, and A. P. Sutton, Phys. Rev. B **57**, 1505 (1998).
[61] P. D. Tepesch, G. D. Garbulsky, and G. Ceder, Phys. Rev. Lett. **74**, 2272 (1995).
[62] G. Ceder, P. D. Tepesch, A. F. Kohan, and A. Van der Ven, J. Electroceram. **1**, 15 (1997).
[63] A. van de Walle and G. Ceder, J. Phase Equilib. **23**, 348 (2002).
[64] G. Ceder, G. D. Garbulsky, and P. D. Tepesch, Phys. Rev. B **51**, 11257 (1995).
[65] N. Metropolis, A. W. Rosenbluth, M. N. Rosenbluth, A. H. Teller, and E. Teller, J. Chem. Phys. **21**, 1087 (1953).
[66] C. Fouassier, G. Matejka, J. M. Reau, and P. Hagenmuller, J. Solid State Chem. **6**, 532 (1973).
[67] J. M. Cowley, J. Appl. Phys. **21**, 24 (1950).
[68] J. Burik, Mater. Sci. Eng., A **324**, 16 (2002).
[69] F. C. Chou, M.-W. Chu, G. J. Shu, F. T. Huang, Woei Wu Pai, H. S. Sheu, T. Imai, F. L. Ning, and Patrick A. Lee, arXiv:0709.0085 (unpublished).
[70] C. A. Marianetti, G. Kotliar, and G. Ceder, Nat. Mater. **3**, 627 (2004).
[71] C. A. Marianetti, G. Kotliar, and G. Ceder, Phys. Rev. Lett. **92**, 196405 (2004).
[72] R. J. Balsys and R. L. Davis, Solid State Ionics **93**, 279 (1997).
[73] I. R. Mukhamedshin, H. Alloul, G. Collin, and N. Blanchard, Phys. Rev. Lett. **93**, 167601 (2004).
[74] Y. Takahashi, Y. Gotoh, and J. Akimoto, J. Solid State Chem. **172**, 22 (2003).
[75] Y. Shao-Horn, L. Croguennec, C. Delmas, E. C. Nelson, and M. A. O'Keefe, Nat. Mater. **2**, 464 (2003).